Differences in Conformational Dynamics between Plasmodium falciparum and Human Hsp90 Orthologues Enable the Structure-Based Discovery of Pathogen-Selective Inhibitors

Wang, Tai; Bisson, William Henry; Mäser, Pascal; Scapozza, Leonardo; Picard, Didier

How to cite

WANG, Tai et al. Differences in Conformational Dynamics between Plasmodium falciparum and Human Hsp90 Orthologues Enable the Structure-Based Discovery of Pathogen-Selective Inhibitors. In: Journal of medicinal chemistry, 2014, vol. 57, n° 6, p. 2524–2535. doi: 10.1021/jm401801t

This publication URL: https://archive-ouverte.unige.ch//unige:35896
Publication DOI: 10.1021/jm401801t

Journal of Medicinal Chemistry

Article

pubs.acs.org/jmc

Differences in Conformational Dynamics between *Plasmodium falciparum* and Human Hsp90 Orthologues Enable the Structure-Based Discovery of Pathogen-Selective Inhibitors

Tai Wang,[†] William H. Bisson,[‡,∥] Pascal Mäser,[§] Leonardo Scapozza,[‡] and Didier Picard*[,†]

[†]Department of Cell Biology, University of Geneva, and [‡]Pharmaceutical Biochemistry Group, School of Pharmaceutical Sciences of the Universities of Geneva and Lausanne, 30 Quai Ernest-Ansermet, CH-1211 Geneva 4, Switzerland

[§]Swiss Tropical and Public Health Institute, University of Basel, Socinstrasse 57, CH-4051 Basel, Switzerland

Supporting Information

ABSTRACT: The high sequence conservation of druggable pockets of closely related proteins can make it challenging to develop selective inhibitors. We designed a new drug discovery approach that exploits both the static and dynamic differences of two orthologues. We applied it, as a proof of concept, to identify compounds that discriminate between the molecular chaperone Hsp90 of the protozoan pathogen *Plasmodium falciparum* (Pf) and that of its human host. We found that the ATP-binding pocket has a Pf-specific extension, whose sequence lining is identical in human Hsp90 but which differs by tertiary structure and dynamics. Using these insights for a structure-based drug screen, we discovered novel 7-azaindole compounds that exclusively bind the recombinant N-terminal domain of PfHsp90 but not of human Hsp90 nor of a PfHsp90 mutant with "human-like" dynamics. Moreover, these compounds preferentially inhibit the growth of yeast complemented by PfHsp90 and block the growth of Pf in culture.

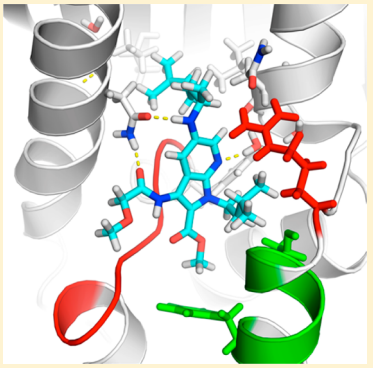

INTRODUCTION

The most severe form of malaria is caused by infections with the protozoan parasite *Plasmodium falciparum* (Pf). Malaria tropica is a serious global health issue that strangles developing countries throughout tropical and subtropical areas. Despite the availability of various classes of drugs that are broadly used for the prevention or the treatment of this disease, eradicating it is challenging and jeopardized by the emergence of drug resistance.[1,2]

The heat shock protein 90 (Hsp90) is a molecular chaperone that ensures the folding, stabilization, and activation of a large spectrum of client proteins such as transcription factors, kinases, E3 ligases, and many other types of proteins involved in a large variety of biological processes.[3−6] Cancer cells are particularly dependent on Hsp90 to maintain protein homeostasis. Hsp90 is therefore regarded as an excellent drug target in oncology.[7−9] Similarly to its buttressing role in cancer cells, Hsp90 appears to support protein homeostasis and protection against stress conditions in protozoan parasites of the genera *Plasmodium*, *Leishmania*, *Trypanosoma*, *Toxoplasma*, and *Eimeria*. They all rely on Hsp90 to provide assistance through the dramatic environmental changes that are imposed on the parasite as it cycles between vectors and mammalian hosts.[10−15] Upon infection by Pf, recurring febrile episodes promote pathogenesis with Hsp90 playing a critical part in buffering repeated heat shocks.[16−18] Systems analysis of molecular chaperone networks suggested that Hsp90 of Pf (PfHsp90) plays a role as a molecular hub for many important factors that are responsible for maintaining the survival and life cycle of the parasite.[19]

The Hsp90 inhibitor geldanamycin (GA) has been demonstrated to arrest the growth of many protozoan pathogens.[10−15,20] In Pf, treatment with GA blocks the transition from the ring to the trophozoite stage during the intraerythrocytic phase of the parasite.[15,16,21] Remarkably, Hsp90 inhibitors appear to be able to cure mice infected with *Trypanosoma evansi*,[20] *Trypanosoma brucei*,[11] and *Plasmodium yoelii*.[22] These previous studies rose the awareness of the scientific community for targeting Hsp90 for the treatment of protozoan infections.[23]

The vast majority of Hsp90 inhibitors are small molecules, which compete with ATP for binding to the N-terminal ATP-binding pocket of Hsp90.[7,9,24] This traps Hsp90 in a conformation resembling the ADP-bound state and consequently blocks Hsp90 function by arresting the dynamic multicomponent cycle.[6,24] Strongly driven by the potential to treat cancer with Hsp90 inhibitors, the development of such inhibitors has rapidly progressed in the last years and there currently exists a broad range of pharmacophores ranging from natural ansamycins to synthetic derivatives of purine, resorcinol, benzamide, aminopyri(mi)dines, and tricyclic imidazopyridines.[9,25,26]

In contrast, the development of species-specific Hsp90 inhibitors is still in its infancy. We previously presented a

Received: November 21, 2013
Published: March 3, 2014

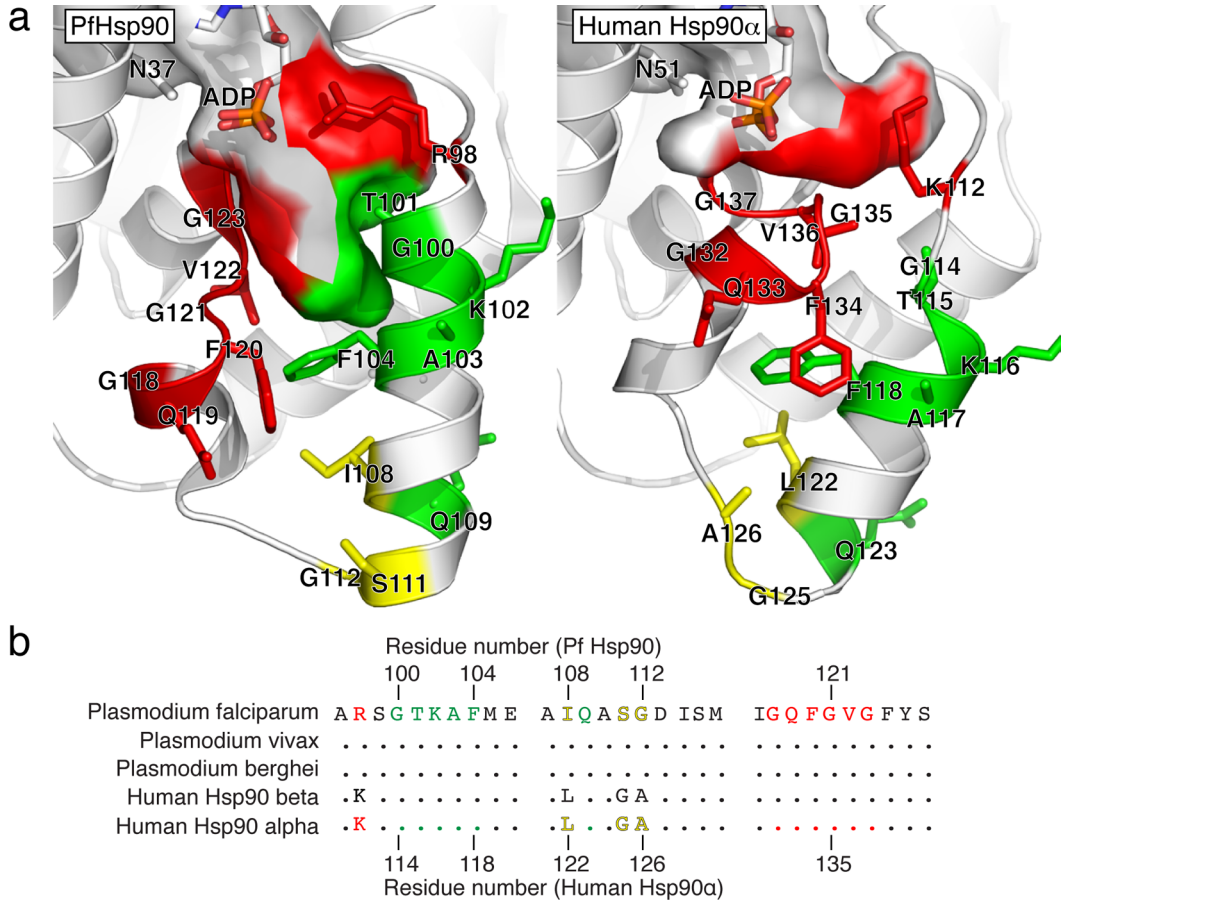

Figure 1. Structure and sequence of a PfHsp90-specific hydrophobic pocket. (a) Comparison of the lid domains between PfHsp90 (PDB 3K60, chain A; left panel) and human Hsp90α (PDB 1BYQ; right panel). Note that the lid is in the open conformation in these and almost all other available structures. The Pf-specific pocket is delimited by the glycine-rich hinge loop (GHL, colored in red in both PfHsp90 and human Hsp90α) and the N-terminal α-helix of the lid domain (colored in green; PfHsp90, G100 to F104; for human Hsp90α, G114 to F118). Hydrophobic pockets, which could accommodate drugs, are represented in solid colors. The surfaces generated by the GHL and by R98 in PfHsp90 and K112 in human Hsp90α are colored in red and those generated by G100 to F104 of PfHsp90 in green. The characteristic IXXSG and LXXGA motifs in the cap of the lid domains of PfHsp90 and human Hsp90s, respectively, are marked in yellow. (b) Sequence alignment of the lid domain of Hsp90. Only residues diverging from those in PfHsp90 are shown. The numbering above and below the alignment is for Pf and human Hsp90α, respectively. The colors of the residues correspond to those of (a).

living test system based on the growth of a panel of isogenic yeast strains, each living on Hsp90 from a different species. Using this system, we demonstrated that already known Hsp90 inhibitors manifest a species selectivity arguing that it might be possible to identify or to design inhibitors with a more pronounced species selectivity.[27] An unbiased biochemical high-throughput screen of over 4000 compounds led to the identification of three additional molecules, including the natural compound harmine, with selective binding to PfHsp90 over human Hsp90.[28] Exploring Hsp90 from pathogens as a drug target is further encouraged by the finding that inhibiting Hsp90 may additionally suppress resistance to other drugs in both pathogenic fungi[29] and protozoans.[17,30] Indeed, Hsp90 inhibition synergizes with the effects of the established antimalarial drug chloroquine (CQ) and even reverses the CQ resistance in Pf cultures.[30,31] Likewise, harmine displays synergy with CQ and artemisinin in vitro and in a mouse model of malaria.[31]

Recently, the crystal structure of ADP-bound PfHsp90 became available,[32] which opened the possibility for structure-based drug screening and design. Notably methods of virtual drug screening (VS)[33,34] make it possible to explore a much larger number of chemotypes and compounds at a fraction of the cost, time and effort required to screen compound libraries with more traditional approaches.[35] Here we describe how we used insights from an in-depth analysis of the structural differences between PfHsp90 and the cytosolic Hsp90 isoforms of the human host for VS and rational drug design. This novel workflow allowed us to exploit a structural difference that is not directly encoded by a primary sequence difference. Through a combination of in silico, in vitro, and in vivo techniques, we identified a novel type of Hsp90 inhibitor with promising selectivity for PfHsp90.

RESULTS

Structural Comparison between Pfhsp90 and Human Hsp90. A structure-based approach for drug discovery requires extensive studies on the specific features of the target protein. We started with the comparison of the protein sequences of Hsp90s between *Plasmodium* and other species (Supporting Information Figure S1a). There are only three residue substitutions inside the ATP-binding pocket between PfHsp90 and human homologues: A38S, R98K, and I173V (Supporting Information Figure S1b). Two of them are difficult

dx.doi.org/10.1021/jm401801t | J. Med. Chem. 2014, 57, 2524−2535

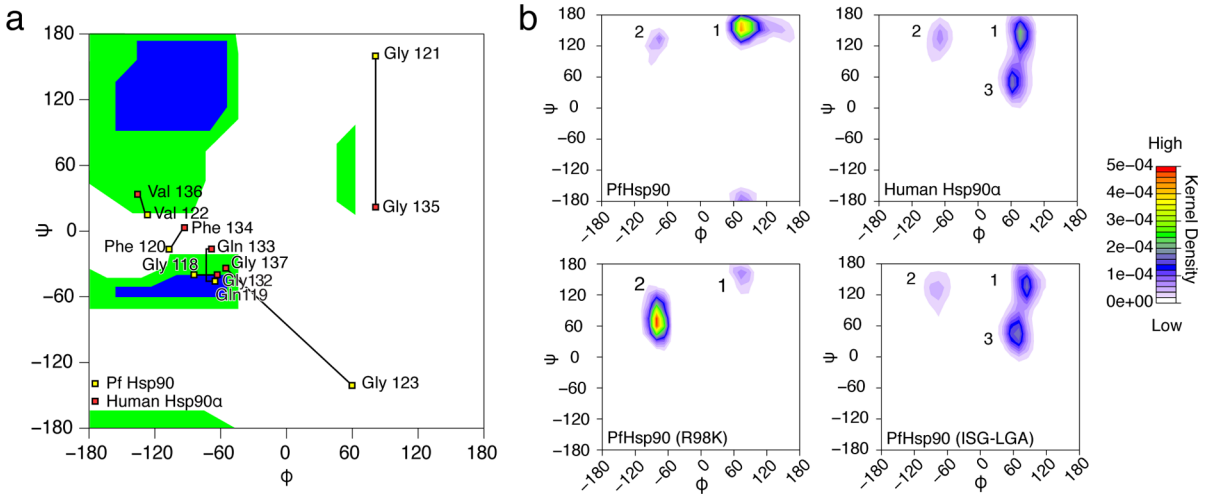

Figure 2. Characterization of the conformational dynamics of the PfHsp90-specific hydrophobic pocket. (a) Ramachandran plot of residues 118 to 123 of PfHsp90 and their human Hsp90α counterparts 132 to 137. Black lines connect the two orthologous residues. (b) Ramachandran plots of the backbone (α-carbon) of G121 along the MD simulation of PfHsp90, its mutant R98K, and its triple mutant ISG-LGA and the corresponding G135 of human Hsp90α (all ligand-free). The enrichment of data points is represented by kernel density in rainbow colors. Conformations 1, 2, and 3 are marked. Conformations 1 and 3 correspond to the ones found in the PfHsp90 and human Hsp90α crystal structures, respectively (see Figure 1a), while the minor conformation 2 may be an intermediate state between conformations 1 and 3.

to exploit for species-specific targeting. A38 is located at the bottom of the ATP pocket, but the residue is only substituted to a serine in the human Hsp90α but not Hsp90β isoform. Moreover, the residue is masked by the structural water molecules (W1 and W4) that mediate the H-bond network between D79 and N37 (Supporting Information Figure S1c).[36] I173 only differs from valine by an extra methyl group, which is unlikely to cause any significant change either to the contour or to the water molecule network of the surrounding inner ATP pocket.

R98K represents a potentially useful difference. The positively charged guanidinium end of the arginine, unlike the lysine side chain, has a planar conformation, allowing not only multiple H-bonds but also binding to aromatic moieties of candidate drugs in a T-shaped or parallel mode through π–cation interactions.[37] However, given the flexibility of the R98 side chain and the hinge region around R98, a useful impact on affinity could only be expected if we hypothesize that the surrounding hydrophobic environment can contribute to accommodate the ligand.

The ATP-binding pocket of Hsp90 is shared by a superfamily of proteins including gyrase, Hsp90, histidine kinase, and MutL.[38] Apart from their characteristic Bergerat fold, there is a flexible domain known as the "ATP lid" (Figure 1a).[38] This lid is connected to two sides of the entrance of the pocket by helices or hinges and linked by a loop at the distal tip. It serves as a rotatable cover that can close over the ATP-binding pocket. The lid domains of the members of this superfamily differ in length, tertiary structure, and the predominance of open/closed states. Upon careful comparison of the sequences and crystal structures of human Hsp90α (PDB 1BYQ) and PfHsp90 (PDB 3K60, chain A), we noticed that the insides of the ATP-binding pockets are nearly identical. In contrast, the conformation of a short hinge at the C-terminal base of the lid displays some significant structural difference (Figure 1a). The hinge contains three glycine residues as part of the motif ***G***QF***G***V***G*** (Figure 1b) and had previously been noticed as a glycine-rich loop in the crystal structure.[32] We will refer to it as the glycine-rich hinge loop (GHL), encompassing residues G118 to G123 in PfHsp90 and G132 to G137 in human Hsp90α (Figure 1a,b). The Ramachandran plot over the residues in the GHL (Figure 2a) revealed that G121 has a much reduced ψ value compared with the human counterpart G135. Moreover, the following glycine G123 has significant shifts in both ψ and φ values compared with the human counterpart G137. This indicates a vastly different conformational flexibility of these two residues. No obvious conformational variation was found further into the lid domain between residues 114 and 120 (Figure 2a and Supporting Information Figure S1d). In both human Hsp90 isoforms (human Hsp90α, PDB 1BYQ; human Hsp90β, PDB 1UYM), the GHL is packed into a curved conformation by which G135 is clipped to G114 at the other end of the lid, resulting in a more compact loop (Figure 1a). In contrast, the distinct geometries of G121 to G123 of PfHsp90 translate into a straight GHL conformation, which disconnects G121 from G100 and opens a new hydrophobic cavity (Figure 1a). This PfHsp90-specific pocket (Pf-specific pocket) is delineated by the GHL and the residues G100, T101, and F104, forming a hydrophobic region under the side chain of R98, which may afford a unique opportunity to design species-selective inhibitors.

Characterization of the Pf-Specific Pocket. Surprisingly, despite the conformational divergence, the sequence of the GHL is 100% conserved (Figure 1b), suggesting that a distant region may impose a different loop structure. A sequence alignment over the lid domain of Hsp90 sequences (Figure 1b and Supporting Information Figure S1a) shows very little variation in both hinge loops (R98 to G104 and G118 to G123), whereas the cap of the lid domain in all *Plasmodium* species features a characteristic IXXSG sequence that marks a clear difference to the LXXGG/A found in human and many other species (Figure 1b, Supporting Information Figure S1a,e). We posited that this sequence might be responsible for the formation of the unique conformation of the GHL in PfHsp90. To support our hypothesis, we performed unbiased molecular dynamics (MD) simulations (over 1000 ns) in solution of ligand-free PfHsp90 (residues 1 to 209), human Hsp90α (residues 5 to 213), a "humanized" PfHsp90 triple mutant

dx.doi.org/10.1021/jm401801t | J. Med. Chem. 2014, 57, 2524−2535

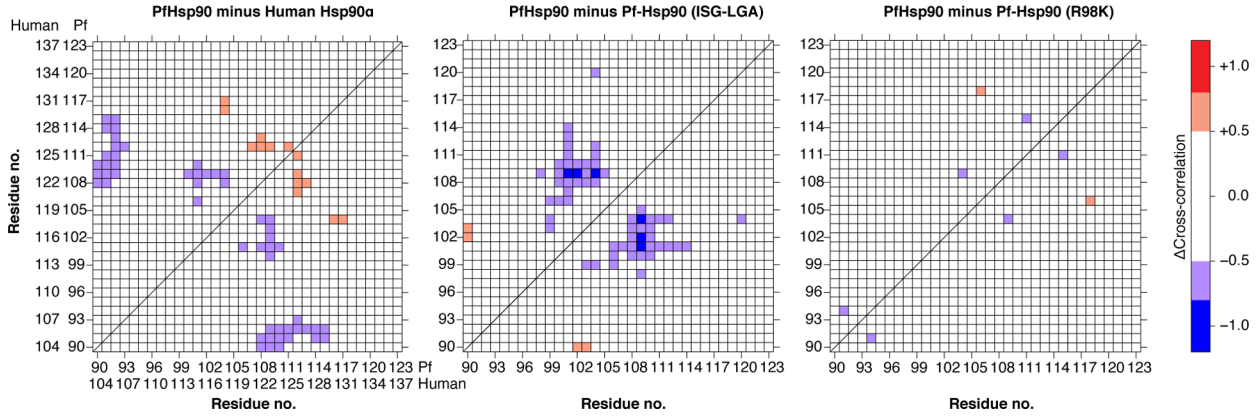

Figure 3. Pairwise comparisons of the cross-correlation matrices of a panel of the indicated Hsp90s.

(I108L, S111G, G112A, hereafter referred to as "ISG-LGA") and PfHsp90 with K98 instead of arginine as in human Hsp90α (R98K). To probe the conformation of the GHL, we focused on the backbone of G121 (of PfHsp90), which is located in the middle of the GHL. Ramachandran plots of G121 along the simulation (Figure 2b) showed that PfHsp90 is predominantly confined to conformation 1 (which corresponds to its conformation in the crystal structure; Figure 2a) and R98K is solely in conformation 2 (Figure 2b). Human Hsp90α exhibits equal distributions over conformations 1 and 3 (the latter corresponds to the one found in the crystal structure; Figure 2), indicating that the human GHL might be more flexible and could dynamically adopt multiple conformations. In accordance with our hypothesis, the "humanized" PfHsp90 mutant ISG-LGA slides between conformations 1 and 3 in a manner very similar to human Hsp90α.

We investigated the cross-correlations of spatial fluctuations of the α-carbons of the polypeptide backbone to further support the hypothesis that it is the distant sequence alteration (ISG-LGA), which contributes to maintaining the Pf-specific pocket open. We generated pairwise dynamic cross-correlation matrices.[39] This analysis informs about the "coordination" of the movements of the polypeptide backbone between pairs of residues during the simulation. Principal component analysis of all pairwise residue cross-correlations over the four Hsp90s (Supporting Information Figure S1f) demonstrated that the mutant ISG-LGA is globally biased to behaving similarly to human Hsp90α, whereas the patterns of PfHsp90 and R98K are more closely related. The comparative analysis of the cross-correlation matrices (Figure 3) highlights the pairwise differences. Over the region close to the lid domain, PfHsp90 R98K, which also serves as a negative control, displays no significant changes in residue cross-correlations (Δcross-correlation between −0.5 and +0.5). More strikingly, the correlation of the backbone movements of Q109 with those of G100 to F104 in PfHsp90 is significantly lower than that of the same residues in the "humanized" PfHsp90 mutant ISG-LGA or that of the equivalent residues in human Hsp90α (between Q123 and G114 to F118) (Figure 3). Hence, the α-helix that extends from the cap to the N-terminal end of the lid domain appears to be more rigid over its entire length in both human Hsp90α and the ISG-LGA mutant. The relative flexibility of the two ends of the α-helix in PfHsp90 and the alternate conformational dynamics of the GHL may be two essential features for preventing the closure of the Pf-specific pocket.

Virtual Drug Screening. On the basis of our more detailed understanding of the Pf-specific pocket, we implemented a structure-based strategy combining multiple layers of virtual drug screening (VS) and modeling to identify Pf-selective candidates (Figure 4 and Supporting Information Figure S2).

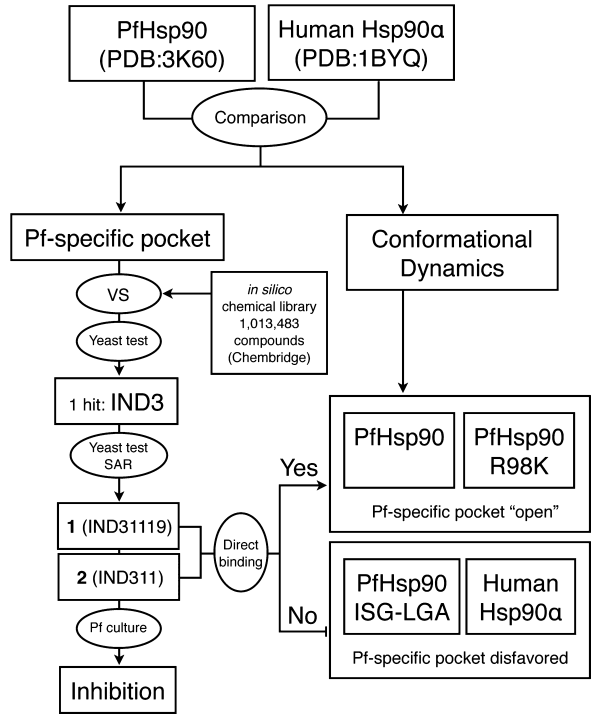

Figure 4. Workflow for the discovery and characterization of **1** and **2**. More details on the steps on the left side (from VS to direct binding assays) are shown in Supporting Information Figure S2. Direct binding assays at the bottom of the scheme connect the left arm of the scheme with the computational analyses of the conformational dynamics of the indicated Hsp90 proteins on the right. SAR, structure−activity relationship analysis.

We performed a VS focusing on the ATP-binding pocket of PfHsp90, which initially generated 10000 top-ranked candidates. To introduce a bias for PfHsp90-selective compounds, these were then rescored into the same model containing the mutations A38S, R98A, and I173V. At this step, we selected the compounds with a significantly decreased docking score for the mutant relative to the wild-type protein. We further refined the results by rescoring the candidates with DOCK 6 AMBER,[40]

dx.doi.org/10.1021/jm401801t | J. Med. Chem. 2014, 57, 2524−2535

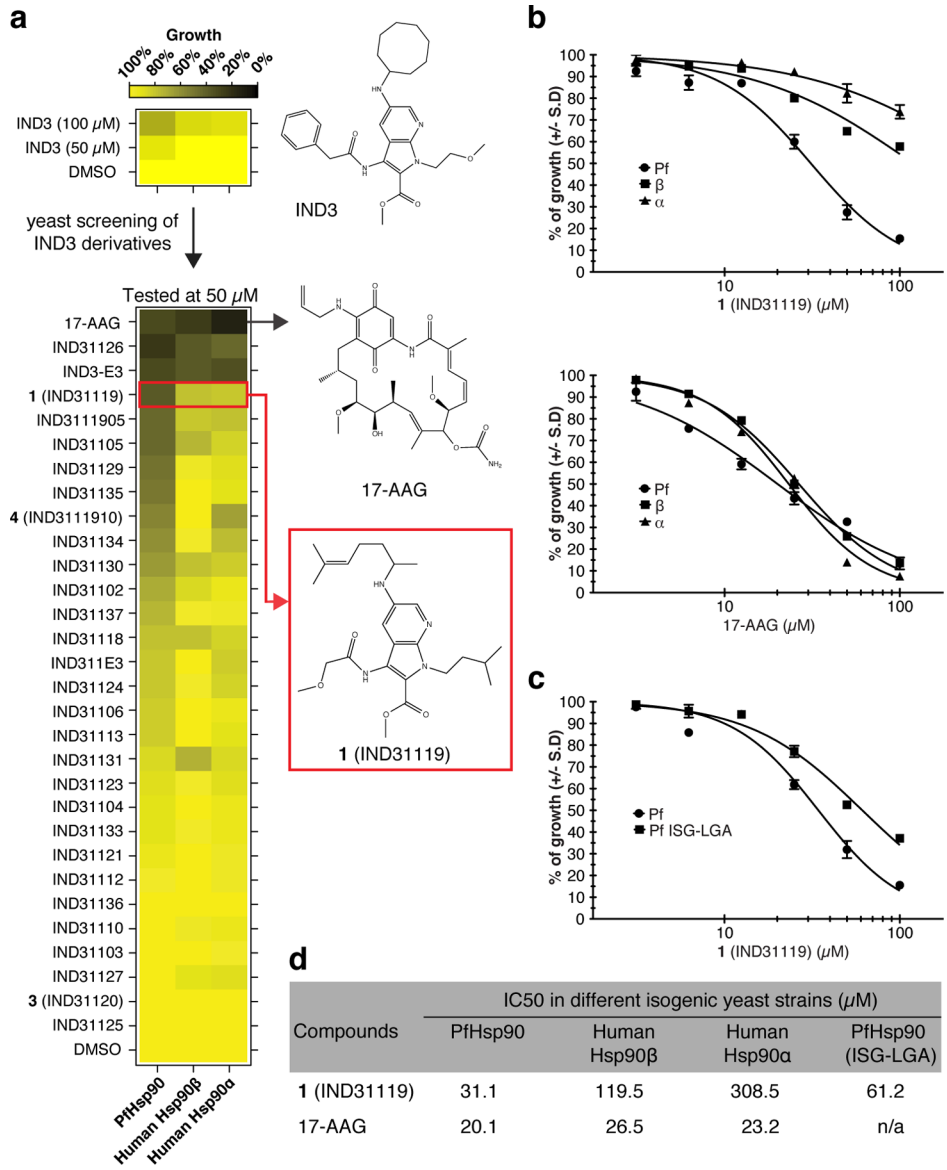

Compounds	IC50 in different isogenic yeast strains (μM)			
	PfHsp90	Human Hsp90β	Human Hsp90α	PfHsp90 (ISG-LGA)
1 (IND31119)	31.1	119.5	308.5	61.2
17-AAG	20.1	26.5	23.2	n/a

Figure 5. Inhibition of growth of yeast tester strains. (a) Heat map of the growth inhibitory effects of the 7-azaindole derivatives of IND3. The reference Hsp90 inhibitor 17-AAG was used for comparison. The results were sorted based on the percentage of growth of the PfHsp90 strain. The structures of the chemicals, estimated errors and numerical values can be found in Supporting Information Figures S3,S4 and Table S1, respectively. (b,c) Dose−response experiments with the indicated strains (PF, PfHsp90; *β*, human Hsp90*β*; *α*, human Hsp90*α*; PF ISG-LGA: PfHsp90$^{ISG-LGA}$) and inhibitors. (d) IC_{50} values of the experiments in (b,c). For simplicity, we omitted the standard deviations of the IC_{50} values, which were 10% or less except for the Hsp90*α* strain treated with **1**.

which allowed the assessment of "induced-fit" effects and a free energy estimation of the ligand binding. The end result of the VS with over a million compounds was five preliminary candidates worth pursuing.

A Panel of Isogenic Yeast Strains as a Tool to Study Hsp90 Inhibition in Vivo. We previously generated a set of isogenic yeast strains that are functionally complemented by plasmid shuffling by Hsp90 from different species, including Pf and human Hsp90*α* and *β*.[27] As wild-type PfHsp90 had been shown to support rather poor growth compared with its human counterparts, we tested the PfHsp90 mutant K313Q. This mutation in human Hsp90 isoforms had previously been reported to mimic the acetylated state of this residue and to improve certain chaperoning functions in yeast.[41] Note that the experimentally mapped acetylation sites of PfHsp90 do not coincide[20] and that this substitution in the middle domain of Hsp90 is not supposed to affect the ligand binding of the N-terminal ATP-binding pocket. Because yeast complemented by the PfHsp90 mutant K313Q grows more robustly, this mutant was used for all subsequent experiments.

We tested all five candidate compounds from the in silico screening with growth assays with the yeast tester set. We found that methyl 5-(cyclooctylamino)-1-(2-methoxyethyl)-3-(2-phenylacetamido)-1*H*-pyrrolo[2,3-*b*]pyridine-2-carboxylate (IND3), a 7-azaindole derivative, showed promising selective growth inhibition at high concentrations (100 *μ*M; see Figure 5a). We next screened a panel of commercially available IND3 derivatives (Supporting Information Figure S3) to identify yet better inhibitors and set the stage for future rational refinements through a structure−activity relationship (SAR) analysis. A graphic representation, error estimation, and the numerical values of the growth assays are given in Figure 5 and

dx.doi.org/10.1021/jm401801t | J. Med. Chem. 2014, 57, 2524−2535

	Binding affinity (Kd in μM)				
	GA (Geldanamycin)	**1** (IND31119)	**2** (IND311)	**3** (IND31120)	**4** (IND3111910)
	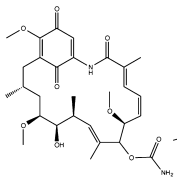	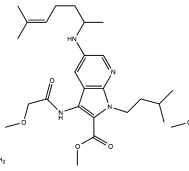	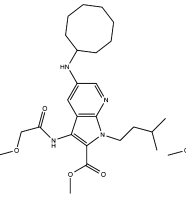	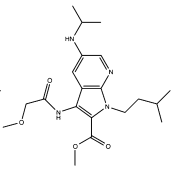	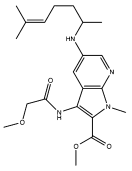
Protein					
PfHsp90	0.318	14.1	25.4	175	115
Human Hsp90β	0.152	NS	NS	NS	
Human Hsp90α	0.714	NS			
PfHsp90 (ISG-LGA)	0.103	NS	NS		
PfHsp90 (R98K)		16.5			

Figure 6. Direct binding assays with purified recombinant proteins. Experiments were performed using microscale thermophoresis and described in the Experimental Section. NS, no detectable binding signal.

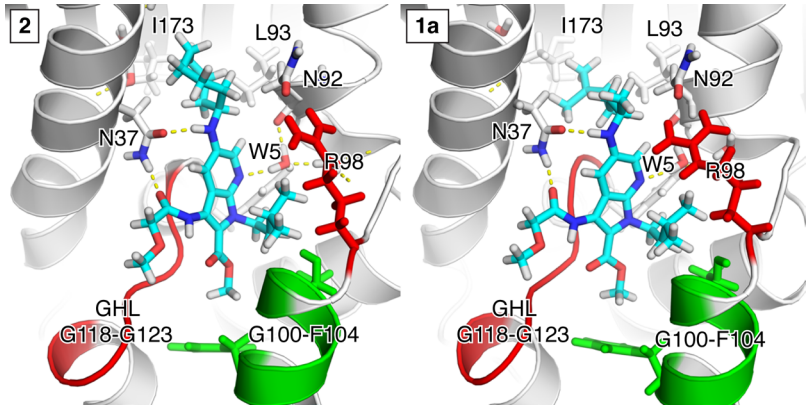

Figure 7. Pose predictions for **1a** and **2** bound to PfHsp90. Models of the poses 1 of compounds **2** (left panel) and **1a** (right panel) in the PfHsp90 drug-binding pocket. H-bonds are illustrated by broken yellow lines. The other colors are as in Figure 1a.

Supporting Information Figure S4 and Table S1, respectively. We found that methyl 1-isopentyl-3-(2-methoxyacetamido)-5-((6-methylhept-5-en-2-yl)amino)-1*H*-pyrrolo[2,3-*b*]pyridine-2-carboxylate (**1**; herein also referred to as IND31119) provides the best selectivity and potency. By comparison to **1**, the established Hsp90 inhibitor 17-allylaminogeldanamycin (17-AAG), an analogue of GA that works in this particular yeast growth assay, inhibits the growth of all three strains without marked selectivity. A few other compounds of the 7-azaindole family also inhibit growth of the tester strains nonselectively. Note that with this type of pattern, it is not possible to exclude that growth is inhibited due to a general cytotoxicity. At this point, our results were compatible with the notion that compounds such as **1** act as direct inhibitors to block PfHsp90 function selectively in vivo.

Direct Binding Assays. Our modeling suggested that the azaindole derivatives bind the N-terminal ATP binding domain of PfHsp90. To provide direct evidence for this hypothesis, we performed binding assays with recombinant purified proteins. These were performed using microscale thermophoresis. Not surprisingly, GA binds PfHsp90 and human Hsp90α and β in a nonselective manner with K_ds of 0.318, 0.714, and 0.152 μM, respectively (Figure 6). In contrast, **1** and its close derivative **2** (IND311) bind exclusively to PfHsp90 with K_ds of 14.1 and 25.4 μM, respectively. Interestingly, upon binding to PfHsp90, GA induces a decrease in the thermophoresis value, whereas **1** and **2** increase it (Supporting Information Figure S5). This behavior suggests that the binding of **1** or **2** provokes a global conformational change of PfHsp90 that is distinct from that induced by GA.

To characterize further the binding mode that accounts for the species selectivity of **1** and **2**, binding to the two more human-like PfHsp90 mutants ISG-LGA and R98K was also examined (Figure 6; see also Figure 4). While R98K retains the ability to bind **1**, ISG-LGA is unable to bind **1** and **2** but displays an even higher affinity for GA. Comparative yeast growth assays with the ISG-LGA mutant further corroborated these findings as the extrapolated IC_{50} for **1** (61 μM compared to 31 μM for wild-type PfHsp90) shifted toward the higher concentrations seen for the human Hsp90s. These results indicated that the selectivity of **1** might stem from the uniquely favored GHL conformation in PfHsp90.

Surprisingly, R98, which is specific for protozoan pathogens, turns out to be dispensable for selectivity and affinity of both GA[20] and our 7-azaindole derivative. Our prediction of the binding poses of **1** and **2** (see below and Figure 7) supports these experimental findings in that R98 merely hovers over the ligand without making any contacts. Considering that our analysis of the GHL conformations predicted an alternate conformation for R98K (Figure 2b), different from those of wild-type PfHsp90 and human Hsp90α, we hypothesize that

dx.doi.org/10.1021/jm401801t | *J. Med. Chem.* 2014, 57, 2524−2535

whatever this dynamically restricted conformation is, it must allow the Pf-specific pocket to stay open.

Prediction of the Binding Pose. We tried to predict the binding pose of the 7-azaindole family of compounds in more detail as a guide for future rational lead optimization. The docking was performed using AutoDock 4.2.[42,43] Because compound **1** contains a chiral center in the side group at the α-carbon at position 5 of the 7-azaindole core, the docking was done with both the *R*- and the *S*-enantiomers (**1a** and **1b**, respectively; see Supporting Information Figure S6a). Six poses for **1a**, **1b**, and **2** were chosen as potential models based on score ranking and conformational population. To evaluate whether these poses were sustainable inside the PfHsp90 binding pocket, we equilibrated the ligand−protein complex by MD for 20 ns with application of harmonic constraints on the α-carbons of the protein. The root-mean-square deviations (RMSD) of the ligands in reference to their original poses were plotted against the nonbond energy calculated between ligand and protein (Supporting Information Figure S6b). It became clear from the analysis that the pose 1 prevails over all others for **1a** as well as **2** for both the degree of cluster density and favorable van der Waals and electrostatic interactions with PfHsp90. The trajectories of the MD indicated that the ligands slide into an optimized pose and stay stably bound in the protein. A prolonged MD simulation of the pose 1 of compound **2** with unconstrained protein backbone also substantiated the robustness (Supporting Information Figure S6c). While the MD simulations with the IND31119 *S*-enantiomer **1b** also suggest that the pose 1 is the most favored one, they indicate substantially reduced stability compared to those of the *R*-enantiomer **1a** (see also below). We therefore speculate that the *R*-enantiomer **1a** may account for all or most of the in vitro and in vivo activities of the racemic mixture.

In the poses 1 of compounds **1a** and **2** (Figure 7 and Supporting Information Figure S7), the 7-azaindole core stays above the characteristic GHL of PfHsp90, and its two side branches at the 1- and 2-positions (Supporting Information Figure S7b), an aliphatic chain and a carboxyl group, respectively, jointly fill the hydrophobic Pf-specific pocket. The amide of N37 pivots about 90°, and the conformation is stabilized by a newly established hydrogen bond between N37 Oδ1 and the secondary amine at the 5-position of the 7-azaindole core. Concomitantly, N37 Nδ2 finds a new H-bond partner with the carbonyl of the amide at the 3-position the 7-azaindole core. This results in the formation of two complementary H-bonds between N37 and **1a** or **2** that are stably maintained along the MD. In addition, we found that a hydrogen bond is established between the 7-position and a structural water molecule (W5, Figure 7) that serves as a hub of H-bonds that connect the backbone of N92, W125, the 7-positions of **1a** or **2** and another structural water molecule that interacts with I96. Interestingly, both water molecules are conserved in the binding modes of GA and ADP, suggesting they represent a set of "integral" structural water molecules of Hsp90.

Key Determinants for Further Derivatization. The predicted binding modes of **1a** and **2** suggested that the group at the 5-position and the aliphatic chain at the 1-position of the 7-azaindole core represent the main decorations that allow space filling of the Pf-specific and inner ATP-binding pockets. They should therefore account for the species-selective affinity. In support of this speculation, the two derivatives **3** (IND31120) and **4** (IND3111910, a racemic mixture) of compound **1**, of which the 5-position and the 1-position are respectively shortened, demonstrated weakened binding (K_ds of 175 and 115 μM, respectively) to PfHsp90 as compared with the one of **1** (K_d = 14.1 μM) (Figure 6). Interestingly, despite different substitutions in the 5-position, the common parts including the 7-azaindole core of **1a** and **2** are predicted to bind very similarly in the Pf-specific pocket (Figure 7 and Supporting Information Figure S7). In contrast, the secondary amine at the 5-position of the 7-azaindole core and the cyclooctyl moiety of **2** are accommodated at the entrance of the inner ATP-binding pocket, and the 6-methylhept-5-en-2-yl chain of **1a** extends even deeper into the ATP-binding pocket where its interactions involve N37, N92, L93, F124, and I173 located on the floor of the ATP-binding pocket (see also Supporting Information Figure S7c). It is noteworthy that I173 is one of the Pf-specific substitutions (I173V), already mentioned above. **1a** provides additional van der Waals interactions with the extra methyl group of I173, which may contribute to the species selectivity of this ligand. The ability of the side group of the enantiomer **1a** to reach further into the ATP-binding pocket might contribute to the overall ligand affinity. The results of the analysis of the other enantiomer, **1b**, are consistent with this hypothesis. Instead of filling the inner part of the ATP-binding pocket as observed with **1a**, the 6-methylhept-5-en-2-yl side chain of **1b** remains in sort of an atrium outside the entrance (Supporting Information Figure S8). Although that may allow additional enthalpic interactions, the MD simulations indicated a much decreased ligand stability. Overall, the 1- and 5-positions of the 7-azaindole core (Supporting Information Figure S7b) might therefore constitute key positions on which further medicinal chemistry should focus.

Inhibition of Pf in Culture. We then tested the effectiveness of our drug candidates to inhibit authentic Pf propagated in culture with human erythrocytes. Using an assay window of 72 h, **1** inhibited the parasite growth with an IC_{50} of about 6 μM (Table 1). Compound **3**, which binds PfHsp90 with lower affinity (Figure 6), displays a higher IC_{50} of about 14 μM. Further supporting the correlation of binding affinity and IC_{50}, GA inhibited the proliferation of Pf with an IC_{50} of 148 nM. Even though we could not measure the binding affinity of these azaindole derivatives for mammalian (human) Hsp90, high concentrations did show a general cytotoxicity in mammalian cells, either because of Hsp90 inhibition or because of other biochemical effects. However, the cytotoxicity values for both derivatives were very close (63 and 56 μM) and more than 10-fold above the IC_{50} for the pathogen.

Table 1. Growth Inhibitory Effects of Selected 7-Azaindole Derivatives and Geldanamycin for *Plasmodium falciparum* in Culture and L6 Cells

compd	*Plasmodium falciparum* in culture IC_{50} (μM ± SD)	L6 cells IC_{50} (μM ± SD)
GA	0.148 ± 0.019	6 ± 5.59
1	5.752 ± 1.889	63 ± 11.31
2	5.022 ± 2.339	56 ± 19.09
3	13.85 ± 1.150	56 ± 7.78

DISCUSSION AND CONCLUSIONS

The vast majority of currently available and tested Hsp90 inhibitors target the N-terminal ATP-binding pocket, clearly

the most druggable domain.[7,8,24] Given the overall very high conservation of Hsp90, we expected that it might be difficult to identify and to design inhibitors that would be selective or even specific for PfHsp90 over the human isoforms. Indeed, the sequence and structural conservation of the ATP-binding pocket is remarkable. The binding of the adenosine moiety of ATP is ensured by a sophisticated H-bond network (Supporting Information Figure S1c), which together form an integral pharmacophore complex. These features are conserved between PfHsp90 and human Hsp90α/β and addressed by nearly all currently developed Hsp90 inhibitors, although it cannot be excluded that new pharmacophores could be lodged into the pocket with different contacts. As discussed above, of the three key residues that differ, essentially only R98 may afford an opportunity to direct drugs specifically at PfHsp90. PfHsp90 shares this residue with all other protozoan parasites that we have analyzed (Supporting Information Figure S1a), which suggests that an inhibitor that exploits this difference might selectively target Hsp90 in many other protozoans that cause other neglected diseases.

Upon examining the available crystal structures in detail, we discovered an area of structural divergence in PfHsp90 that arises without underlying sequence divergence. In PfHsp90, the GHL situated at one of the hinges of the lid at the entrance of the ATP-binding pocket adopts a unique extended conformation. This contributes to opening up a Pf-specific pocket, which drug screening and rational design may be able to exploit. Our MD analyses predicted that this conformational difference could be due to a species-specific sequence motif located in the cap of the lid, a region that is not in proximity or direct contact with the Pf-specific pocket. The motif IXXSG, and hence possibly its remote conformational impact, constitutes a *Plasmodium*-specific feature that is completely conserved across a broad range of *Plasmodium* strains and species (Supporting Information Figure S1a,e). In addition, the MD simulations indicated another impact of the motif IXXSG. We observed an increased correlation of the backbone fluctuations between Q109 and G100 to F104 when the sequence was mutated in silico into the human motif LXXGA (Figure 3). Interestingly, the invariant residue Q109 is located within the sequence motif and G100 to F104 are part of an α-helix that contributes to delimiting the Pf-specific pocket in close vicinity to the GHL (Figure 1a). The MD simulations also predicted that the conformation of the GHL in wild-type PfHsp90 is more uniform and more constrained compared with that of human Hsp90α and that the integrity of the Pf-specific pocket is compromised by changing the three residues of the *Plasmodium*-specific motif to that of human Hsp90 (Figure 2b).

Thus, our structural and computational discoveries led us to conclude that the minor primary sequence differences between the human and *Plasmodium* Hsp90s translate into far more important structural differences and that these could form the basis for a VS. The screen for PfHs90-selective compounds from a very large and diverse library yielded an entirely new pharmacophore that indeed appears to use the Pf-specific pocket. We found by computational methods for **1** and **2**, two of the more advanced derivatives of the original 7-azaindole identified by VS, that these compounds might prefer a pose that takes advantage of this pocket. Most importantly, we extended these computational analyses by providing strong experimental support for this model with in vitro and in vivo experiments. 7-Azaindole derivatives selectively bind PfHsp90 in vitro, and this depends on the IXXSG motif and thus presumably the corresponding conformation of the lid. Likewise, these compounds inhibit the proliferation of yeast cells whose viability is maintained by wild-type PfHsp90 but not the IXXSG mutant. Collectively, our data predict the structural model shown in Figure 7 that will ultimately have to be proven or refined by determining an experimental structure.

The strength of our approach is that it takes advantage of conformational differences that may be apparent in static crystal structure, but even more so upon comparing dynamic properties. It is not that human Hsp90s, and the IXXSG mutant of PfHsp90 for that matter, cannot at all adopt the conformation that is favored by PfHsp90. They can, but ligand binding is entropically penalized when the GHL conformation is not constrained. As a result, the species selectivity of our current compounds is primarily due to a thermodynamic difference in binding to PfHsp90 compared to human Hsp90s.

Our currently best inhibitors bind PfHsp90 with moderate affinity and species selectivity and inhibit yeast tester strains with moderate selectivity and IC_{50}s comparable to that of 17-AAG. Importantly, they do inhibit authentic Pf in culture with IC_{50}s in the μM range, a concentration about 10-fold lower than that seen for general cytotoxicity but considerably higher than that of the reference compound GA. It should be noted that our experiments with the racemic mixture of **1** may have overestimated the K_d and IC_{50} and that the real values may be even more favorable for enantiomer **1a**. While these results demonstrate that our drug discovery pipeline is able to exploit minor primary sequence differences, they do emphasize the importance of further improvements by rational drug design and medicinal chemistry to convert exciting hits into drugs. If the general cytotoxicity toward mammalian cells could be maintained, essentially only a 4-fold improvement over **1** in potency toward PfHsp90 would match the cytotoxicity/potency ratio of GA, and lowering the K_d toward that of GA (or 17-AAG) would yield a potentially sufficient therapeutic discrimination between the pathogen and its human host. Even focusing on compound **1**-related 7-azaindoles, this could be achieved by a combination of unbiased screening and rational drug design. New compounds should ideally combine two pharmacophores: one that interacts with the Pf-specific pocket close to the GHL, and perhaps with R98, to confer species selectivity and another that fits into the canonical inner ATP-binding pocket to impart high affinity.

Compound **1** represents a first-generation compound discovered to be selective for an essential pathogen protein over the orthologous protein of the human host. Absolute selectivity might not be necessary considering that some toxicity might be tolerable for the short-term treatment of a potentially lethal acute disease such as malaria. In oncology, one attempts to exploit a therapeutic window between the increased sensitivity of cancer cells to Hsp90 inhibitors and the general cytotoxicity of these molecules, except for the fact that a long-term treatment is likely to be necessary.[7,8] More recently, there is an increasing awareness that combination therapies with Hsp90 inhibitors against cancer might be more successful and possibly associated with less toxicity.[24] By analogy, combination therapies might also be the way to go to treat protozoan diseases. Interestingly, the treatment of Pf cultures with a general histone deacetylase inhibitor potentiates the growth inhibitory effects of GA,[20] and a recent study shows that PfHsp90 directly interacts with the CQ resistance transporter, perhaps explaining in part how inhibition of PfHsp90 can reverse CQ resistance.[30] It cannot formally be excluded that

mutations could arise that would render PfHsp90 resistant to inhibitors. Even though a stepwise selection with an Hsp90 inhibitor led to such a mutation on the backside of the ATP-binding pocket,[28] the synergy with chloroquine was maintained[30] and it is not clear whether viability of the mutant during a normal life cycle would be compromised. Moreover, rendering the "drug binding pocket" itself resistant to an inhibitor through mutation is not particularly probable considering that ATP binding and hydrolysis by the very same pocket are essential for viability.[44]

Our discovery of a promising new pharmacophore constitutes a proof of concept for our novel workflow. The detailed scrutiny of the target protein allowed us to set up a large-scale in silico screen for compounds that could take advantage of a Pf-specific hydrophobic pocket. The analysis of the differences in conformational dynamics done in parallel set the stage for predicting the binding site and explaining the species selectivity of compounds that came out of the VS and experimental pipeline. Demonstrated here for two orthologous proteins, this concept may be more generally applicable, notably to closely related proteins of the same species. In drug screens, conformationally constrained mutants could help to eliminate compounds that target closely related unwanted targets.

EXPERIMENTAL SECTION

Reagents. GA was purchased from LC Laboratories, 17-AAG from Sigma-Aldrich, and the 7-azaindole compounds from Chembridge (San Diego, CA). The structures and 99% purity of the tested 7-azaindole compounds were confirmed by Chembridge using LC/MS. Several compounds such as **1** and **4** could only be obtained as racemic mixtures, which were used for all growth and binding assays. All chemicals were dissolved in 100% DMSO to 10 mM and stored at −20 °C.

Virtual Drug Screening. The in silico library (Chembridge) containing 1013483 compounds was downloaded from the ZINC database (zinc.docking.org).[45] The protein model of PfHsp90 was obtained from the crystal structure of PfHsp90 (PDB 3K60, chain A).[32] Solvent and ligand were removed, and structural water W1 (Supporting Information Figure S1c) was conserved. The model was minimized for 1000 steps (steepest descent) before generation of the grid and spheres in the DOCK 6 package (UCSF). The screening was performed using DOCK 6.3 (UCSF) on an IBM BlueGene/P computer allocating 1024 virtual cores. The 10000 top ranked candidates were rescored in the same model bearing the A38S, R98A, and I173V mutations, generating a selective bias toward PfHsp90. As a control, ADP was docked into the same model; it ranked at 5487 out of 1013483 compounds. There were 390 candidates that displayed a decrease of grid score greater than 8. They were rescored with the DOCK 6 AMBER package.[40] The top 200 of these were manually inspected in Chimera (UCSF)[46] for close proximity with R98 and fitting in the Pf-specific pocket. The five top candidates were purchased for further analyses.

Molecular Dynamics. The models (PfHsp90, PfHsp90^{R98K}, PfHsp90$^{ISG-LGA}$, human Hsp90α) were obtained from the crystal structures: for PfHsp90, PDB 3K60, chain;[32] for human Hsp90α, PDB 1BYQ.[36] Mutations were made in silico with Chimera[46] using the "Rotamers" tool. Ligands were removed, and the rest of the structures (including structural waters) were parametrized by FF11 from AMBER11.[47] A solvent box of 8 Å was generated around the proteins in the presence of counterions to equilibrate the charges. The models were first minimized in ACEMD[48] for 250 steps, followed by 1 ns NVE (300K, with harmonic constraints on the α-carbons) and 2 ns NPT (without the harmonic constraints, Langevin damping at 1 ps^{-1}). Production MD was performed in ACEMD at 300K for 1000 ns (NVT) with a cutoff of 9.5 Å, constrained H-bonds, time step of 4 fs, Langevin damping at 0.1 ps^{-1}, and a PME frequency of 2 fs.

Studies of the GHL conformations: Ramachandran plots of G121 (PfHsp90, PfHsp90^{R98K}, PfHsp90$^{LSG-LGA}$) or of the corresponding residue G135 (human Hsp90α) were generated using the Bio3d package in R[39] based on the trajectories from the aforementioned production MD with omission of the first 200 ns. Kernel density of the data points was calculated with the MASS package and plotted with the lattice package in R.[49,50]

Generation of the pairwise dynamic cross-correlation matrices: The trajectories of the α-carbons from the production MD (of PfHsp90, PfHsp90^{R98K}, PfHsp90$^{ISG-LGA}$, and human Hsp90α) were extracted and analyzed in R using the dccm tool from the Bio3d package.[39] Each matrix in Figure 3 was generated by subtracting from the cross-correlation matrix of PfHsp90 those of human Hsp90α or of the PfHsp90 mutants ISG-LGA or R98K. Grids were generated with the lattice package in R.[50]

Prediction of the Binding Poses. The models of the *R*- and *S*-enantiomers **1a** and **1b**, respectively, of IND31119 and of compound **2**, and of PfHsp90 (ligand- and solvent-free, W1 kept), were charged by Gasteiger charges in MGLTOOLS.[43] Docking was performed using the Lamarckian generic algorithm in Autodock 4.2.[42,43] The algorithm was first tested to ensure that experimentally known poses for Hsp90 inhibitors could be reproduced. For compounds **1a**, **1b**, and **2**, six poses of each molecule were selected based on the conformational population and docking scores and parametrized by GAFF in the AMBER11 package.[47] The protein model (W1 kept) was parametrized by FF11 from AMBER11 and then assembled with the ligand. A solvent box of 8 Å was generated around the complex in the presence of counterions to equilibrate the charges. The models were first minimized in ACEMD for 250 steps, followed by 1 ns NVE and 20 ns NPT (300K, with harmonic constraints on α-carbons of the protein with a cutoff of 9.5 Å, constrained H-bonds, time step of 2 fs, Langevin damping at 1 ps^{-1}, and a PME frequency of 2 fs). The protein was aligned in the trajectory before calculating the RMSD of the ligand. Nonbond energy between protein and ligand was calculated using the "Energy tool" in VMD.[51] The RMSD of the ligand was plotted against the nonbond energy for each trajectory frame of the MD, and kernel density of the data points was represented as a gradient of rainbow colors (generated by the MASS and lattice packages in R).[49,50] The models for the poses 1 of compounds **1a** and **2** (Figure 7) and **1b** (Supporting Information Figure S8) were generated by taking the last frame of the 20 ns MD simulation (NPT) described above, followed by 20000 steps of energy minimization ("conjugate gradient" in UCSF Chimera).[46,47] Prolonged MD (3000 ns NVT, 300K, time step of 4 fs, Langevin damping at 0.1 ps^{-1}; with ACEMD) was performed on pose 1 of compound **2** (restarted from the 20 ns MD NPT) according to the procedures described above but without harmonic constraints.

Plasmids. Yeast vectors: All Hsp90s were expressed from low copy number plasmids with N-terminal Flag tags. The vectors expressing human Hsp90s have been previously described.[27] The mutation for PfHsp90^{K313Q} was generated by PCR site-directed mutagenesis with in subclone of PfHsp90 using a pair of complementary primers covering the mutation site: ....AAACAACAGCCATTAT... and ....TATTTGTTGTCGGTAATAC... (the mutations are underlined), before recloning the open reading frame back into the yeast expression vector pHGF[27] between the *Bam*HI and *Sal*I sites. The plasmid for PfHsp90^{R98K}, a precursor for the pRSET construct mentioned below, was similarly generated using the two complementary primers ...ATTGCAAAGTCAGGAAC... and ...GTTCCTGACTTTGCAA-TAG... . The expression vector for the mutant PfHsp90$^{ISG-LGA}$ was obtained by site-directed mutagenesis of the plasmid pHGF/PfHsp90^{K313Q} by a commercial service (Mutagenex).

Protein expression vectors: The N-terminal ATP-binding domains (residues 1 to 223) of PfHsp90, human Hsp90β, human Hsp90α, PfHsp90$^{ISG-LGA}$, and PfHsp90^{R98K} were cloned from the pHGF vectors into expression vector pRSET A (Life Technologies) using PCR with primers generating ends containing *Bam*HI and *Eco*RI sites (for PfHsp90s, GATCTGGGGATCCATGTCAACGGAAACATTCGC and GGGAATTCTGCAGCTATTCTTCTTCAGATGC) or *Bam*HI and *Pst*I sites (for human Hsp90β, GATCTGGGGATCCATGCCT-GAGGAAGTGCACCA and GGGAATTCTGCAGC-

dx.doi.org/10.1021/jm401801t | J. Med. Chem. 2014, 57, 2524−2535

TACTTCTCTCGTTCCTT; for human Hsp90α, GATCTGGGGATCCATGCCTGAGGAAACCCAGAC and GGGAATTCTGCAGCTACTCCACAAAAAGAGT). The restriction sites are underlined.

Protein Expression. The proteins were expressed in *Escherichia coli* strain BL21 DE3 pLysS grown in LB medium. The expression of wild-type and mutant variants of PfHsp90 was induced with 0.5 mM IPTG for 18 h at 20 °C and the expression of human Hsp90s 37 °C for 4 h. Cells were centrifuged and resuspended in lysis buffer (20 mM HEPES, pH 7.4, 20 mM imidazole, 100 mM NaCl) supplemented with 1× EDTA-free protease inhibitor cocktail (Roche). Cells were lysed with a French press and cell debris removed by centrifugation. The proteins were affinity purified on a HisTrap FF column (GE Healthcare Life Sciences), followed by size exclusion chromatography on a Superdex 200 10/30 GL column (GE Healthcare Life Sciences) by collecting only the fractions of 33 kDa. The purified proteins were concentrated for subsequent experiments using Amicon Ultra-15 centrifugal filters (Millipore) in 20 mM HEPES, pH 7.4, 100 mM NaCl.

Direct Binding Assays. The purified proteins were labeled with the Monolith NT.115 protein labeling kit (NanoTemper Technologies) following the manufacturer's instructions and eluted in 50 mM Tris-HCl pH 7.4, 150 mM NaCl, 10 mM $MgCl_2$, 0.05% Tween-20. Chemicals were titrated in 1:1 dilutions. Direct binding assays were performed by microscale thermophoresis with a Monolith NT.115 microscale (NanoTemper Technologies) using hydrophilic capillaries with 100 nM protein and 5% DMSO at 40% LED power and 40% MST power.

Yeast Test System. All yeast strains were derived from strain DP533,[27] which has the following genotype: *MATa ade2-101-o his3-Δ200 leu2-3,112 lys2-801-a trp1-289 ura3-52 Δhsc82::KanMx4 Δhsp82::KanMx4, pdr5::Leu2/2 μ-HSC82-URA3.* To generate the isogenic yeast strains used in this paper, transformants of DP533 were obtained with plasmids pHGF/PfHsp90^{K313Q}, pHGF/HsHsp90β, pHGF/HsHsp90α, or pHGF/PfHsp90$^{ISG\text{-}LGA,\ K313Q}$ by selection on plates without histidine and then cured of the episome *2μ-HSC82-URA3* by growth on plates containing 5-fluoroorotic acid.

For growth assays, cultures were diluted to an OD600 of 0.1 in minimal medium. Chemicals were first pipetted into a transparent 96-well plate (the wells on the boarder were omitted and filled with 200 μL H_2O) and then diluted with 200 μL of yeast culture suspension to a final drug concentration of 50 μM (2% DMSO). In these assays, 17-AAG was used instead of GA because we found that the latter does not work in minimal medium under these conditions. Growth was recorded with a Sunrise 96-well plate-reader (Tecan) programmed to read OD600 every 30 min for 72 h in total. Data were generated in duplicates for screening or in triplicates for measuring IC_{50} values. The maximal slope of the growth curve was determined and the percentage of the growth was calculated by dividing the maximal slope in drug-treated samples over those treated with solvent alone.

In Vitro Antimalarial Activity and Cytotoxicity. *Pf* strain NF54 was cultured according to Trager and Jensen (ref 52 and www.mr4.org). IC_{50} values were determined in vitro by measuring incorporation of the nucleic acid precursor [^{3}H]hypoxanthine.[53] Cytotoxicity was assessed in L6 cells, a primary cell line derived from rat skeletal myoblasts, as described elsewhere.[54]

■ ASSOCIATED CONTENT

Ⓢ Supporting Information

Additional figures and table with more extensive sequence and structural analyses, details on the VS workflow, chemical structures of the tested 7-azaindole derivatives, statistics of yeast assays, primary data of the in vitro binding assays, further details about pose predictions, additional models for both enantiomers, and numerical values of the yeast growth assays. This material is available free of charge via the Internet at http://pubs.acs.org.

■ AUTHOR INFORMATION

Corresponding Author

*Phone: +41 22 379 6813. Fax: +41 22 379 6928. E-mail: didier.picard@unige.ch.

Present Address

‖For W.H.B.: Environmental Health Sciences Center, Department of Environmental and Molecular Toxicology, Oregon State University, Corvallis, Oregon 97331, United States.

Author Contributions

T.W. and D.P. designed the study and wrote the manuscript; T.W. performed most of the experiments; P.M. supervised and analyzed the Pf culture experiments; W.H.B. and L.S. helped with the design of the computational analyses and guided them; T.W. and D.P. analyzed all of the data; all authors commented on the manuscript.

Notes

The authors declare no competing financial interest.

■ ACKNOWLEDGMENTS

We are indebted to Utpal Tatu and to Rishi Kumar from his lab (IIS, Bangalore, India) for performing and helping with pilot binding assays early in the project and to Dylan Pillai and Dea Shahinas (of the University of Toronto at that time) for collaborating during the initial stages of the project. We are grateful to the Center for Advanced Modeling Science (CADMOS) for providing access to the IBM BlueGene/P for the virtual drug screening. We thank Pierre Dupuis for his contribution to compiling Perl scripts that facilitated sorting, comparison, and extraction of the massive data from the virtual screening, Diana Wider from the DP lab for technical assistance on related aspects of the project, Sibylle Sax from the PM lab for technical assistance, and Leonardo Lauciello from the LS lab for sharing his experience with protein purification and binding assays. An R'Equip grant from the Swiss National Science Foundation (SNF) and the Boninchi Foundation supported the purchase of the microscale thermophoresis instrument. The project was further supported by other grants from the SNF, the Indo−Swiss Joint Research Programme and the Boninchi Foundation, and by the Canton de Genève.

■ ABBREVIATIONS USED

CQ, chloroquine; GA, geldanamycin; GHL, glycine-rich hinge loop; Hsp90, heat shock protein 90; MD, molecular dynamics; Pf, *Plasmodium falciparum*; RMSD, root-mean-square deviations; SAR, structure−activity relationship; VS, virtual drug screening

■ REFERENCES

(1) Hyde, J. E. Drug-resistant malaria—an insight. *FEBS J.* **2007**, *274*, 4688−4698.

(2) Ridley, R. G. Medical need, scientific opportunity and the drive for antimalarial drugs. *Nature* **2002**, *415*, 686−693.

(3) Taipale, M.; Jarosz, D. F.; Lindquist, S. HSP90 at the hub of protein homeostasis: emerging mechanistic insights. *Nature Rev. Mol. Cell. Biol.* **2010**, *11*, 515−528.

(4) Echeverría, P. C.; Bernthaler, A.; Dupuis, P.; Mayer, B.; Picard, D. An interaction network predicted from public data as a discovery tool: application to the Hsp90 molecular chaperone machine. *PLoS One* **2011**, *6*, e26044.

(5) Picard, D. Preface to Hsp90. *Biochim. Biophys. Acta* **2012**, *1823*, 605−606.

(6) Röhl, A.; Rohrberg, J.; Buchner, J. The chaperone Hsp90: changing partners for demanding clients. *Trends Biochem. Sci.* **2013**, *38*, 253−262.
(7) Whitesell, L.; Lin, N. U. HSP90 as a platform for the assembly of more effective cancer chemotherapy. *Biochim. Biophys. Acta* **2012**, *1823*, 756−766.
(8) Jhaveri, K.; Taldone, T.; Modi, S.; Chiosis, G. Advances in the clinical development of heat shock protein 90 (Hsp90) inhibitors in cancers. *Biochim. Biophys. Acta* **2012**, *1823*, 742−755.
(9) Wang, T.; Echeverria, P. C.; Picard, D. Overview of molecular chaperones in health and disease. In *Inhibitors of Molecular Chaperones As Therapeutic Agents*; Machajewski, T. D., Gao, Z., Eds.; RSC Publishing: Cambridge, U.K., 2013.
(10) Peroval, M.; Pery, P.; Labbe, M. The heat shock protein 90 of *Eimeria tenella* is essential for invasion of host cell and schizont growth. *Int. J. Parasitol.* **2006**, *36*, 1205−1215.
(11) Meyer, K. J.; Shapiro, T. A. Potent antitrypanosomal activities of heat shock protein 90 inhibitors in vitro and in vivo. *J. Infect. Dis.* **2013**, *208*, 489−499.
(12) Wiesgigl, M.; Clos, J. Heat shock protein 90 homeostasis controls stage differentiation in *Leishmania donovani*. *Mol. Biol. Cell* **2001**, *12*, 3307−3316.
(13) Echeverría, P. C.; Matrajt, M.; Harb, O. S.; Zappia, M. P.; Costas, M. A.; Roos, D. S.; Dubremetz, J. F.; Angel, S. O. *Toxoplasma gondii* Hsp90 is a potential drug target whose expression and subcellular localization are developmentally regulated. *J. Mol. Biol.* **2005**, *350*, 723−734.
(14) Roy, N.; Nageshan, R. K.; Ranade, S.; Tatu, U. Heat shock protein 90 from neglected protozoan parasites. *Biochim. Biophys. Acta* **2012**, *1823*, 707−711.
(15) Banumathy, G.; Singh, V.; Pavithra, S. R.; Tatu, U. Heat shock protein 90 function is essential for *Plasmodium falciparum* growth in human erythrocytes. *J. Biol. Chem.* **2003**, *278*, 18336−18345.
(16) Pavithra, S. R.; Banumathy, G.; Joy, O.; Singh, V.; Tatu, U. Recurrent fever promotes *Plasmodium falciparum* development in human erythrocytes. *J. Biol. Chem.* **2004**, *279*, 46692−46699.
(17) Shonhai, A. Plasmodial heat shock proteins: targets for chemotherapy. *FEMS Immunol. Med. Microbiol.* **2010**, *58*, 61−74.
(18) Udomsangpetch, R.; Pipitaporn, B.; Silamut, K.; Pinches, R.; Kyes, S.; Looareesuwan, S.; Newbold, C.; White, N. J. Febrile temperatures induce cytoadherence of ring-stage *Plasmodium falciparum*-infected erythrocytes. *Proc. Natl. Acad. Sci. U. S. A.* **2002**, *99*, 11825−11829.
(19) Pavithra, S. R.; Kumar, R.; Tatu, U. Systems analysis of chaperone networks in the malarial parasite *Plasmodium falciparum*. *PLoS Comput. Biol.* **2007**, *3*, 1701−1715.
(20) Pallavi, R.; Roy, N.; Nageshan, R. K.; Talukdar, P.; Pavithra, S. R.; Reddy, R.; Venketesh, S.; Kumar, R.; Gupta, A. K.; Singh, R. K.; Yadav, S. C.; Tatu, U. Heat shock protein 90 as a drug target against protozoan infections: biochemical characterization of HSP90 from *Plasmodium falciparum* and *Trypanosoma evansi* and evaluation of its inhibitor as a candidate drug. *J. Biol. Chem.* **2010**, *285*, 37964−37975.
(21) Kumar, R.; Musiyenko, A.; Barik, S. The heat shock protein 90 of *Plasmodium falciparum* and antimalarial activity of its inhibitor, geldanamycin. *Malar. J.* **2003**, *2*, 30.
(22) Mout, R.; Xu, Z. D.; Wolf, A. K.; Jo Davisson, V.; Jarori, G. K. Anti-malarial activity of geldanamycin derivatives in mice infected with *Plasmodium yoelii*. *Malar. J.* **2012**, *11*, 54.
(23) Dolgin, E.; Motluk, A. Heat shock and awe. *Nature Med.* **2011**, *17*, 646−649.
(24) Neckers, L.; Workman, P. Hsp90 molecular chaperone inhibitors: are we there yet? *Clin. Cancer Res.* **2012**, *18*, 64−76.
(25) Vallée, F.; Carrez, C.; Pilorge, F.; Dupuy, A.; Parent, A.; Bertin, L.; Thompson, F.; Ferrari, P.; Fassy, F.; Lamberton, A.; Thomas, A.; Arrebola, R.; Guerif, S.; Rohaut, A.; Certal, V.; Ruxer, J. M.; Gouyon, T.; Delorme, C.; Jouanen, A.; Dumas, J.; Grépin, C.; Combeau, C.; Goulaouic, H.; Dereu, N.; Mikol, V.; Mailliet, P.; Minoux, H. Tricyclic series of heat shock protein 90 (Hsp90) inhibitors part I: discovery of tricyclic imidazo[4,5-*c*]pyridines as potent inhibitors of the Hsp90 molecular chaperone. *J. Med. Chem.* **2011**, *54*, 7206−7219.
(26) Roughley, S. D.; Hubbard, R. E. How well can fragments explore accessed chemical space? A case study from heat shock protein 90. *J. Med. Chem.* **2011**, *54*, 3989−4005.
(27) Wider, D.; Peli-Gulli, M. P.; Briand, P. A.; Tatu, U.; Picard, D. The complementation of yeast with human or *Plasmodium falciparum* Hsp90 confers differential inhibitor sensitivities. *Mol. Biochem. Parasitol.* **2009**, *164*, 147−152.
(28) Shahinas, D.; Liang, M.; Datti, A.; Pillai, D. R. A repurposing strategy identifies novel synergistic inhibitors of *Plasmodium falciparum* heat shock protein 90. *J. Med. Chem.* **2010**, *53*, 3552−3557.
(29) Cowen, L. E. The fungal Achilles' heel: targeting Hsp90 to cripple fungal pathogens. *Curr. Opin. Microbiol.* **2013**, *16*, 377−384.
(30) Shahinas, D.; Folefoc, A.; Taldone, T.; Chiosis, G.; Crandall, I.; Pillai, D. R. A purine analog synergizes with chloroquine (CQ) by targeting Hsp90 (PfHsp90). *PLoS One* **2013**, *8*, e75446.
(31) Shahinas, D.; Macmullin, G.; Benedict, C.; Crandall, I.; Pillai, D. R. Harmine is a potent antimalarial targeting Hsp90 and synergizes with chloroquine and artemisinin. *Antimicrob. Agents Chemother.* **2012**, *56*, 4207−4213.
(32) Corbett, K. D.; Berger, J. M. Structure of the ATP-binding domain of *Plasmodium falciparum* Hsp90. *Proteins* **2010**, *78*, 2738−2744.
(33) Schneider, G.; Fechner, U. Computer-based de novo design of drug-like molecules. *Nature Rev. Drug Discovery* **2005**, *4*, 649−663.
(34) Bisson, W. H. Editorial: computational chemogenomics in drug design and discovery. *Curr. Top. Med. Chem.* **2012**, *12*, 1867−1868.
(35) Guiguemde, W. A.; Shelat, A. A.; Bouck, D.; Duffy, S.; Crowther, G. J.; Davis, P. H.; Smithson, D. C.; Connelly, M.; Clark, J.; Zhu, F.; Jimenez-Diaz, M. B.; Martinez, M. S.; Wilson, E. B.; Tripathi, A. K.; Gut, J.; Sharlow, E. R.; Bathurst, I.; El Mazouni, F.; Fowble, J. W.; Forquer, I.; McGinley, P. L.; Castro, S.; Angulo-Barturen, I.; Ferrer, S.; Rosenthal, P. J.; Derisi, J. L.; Sullivan, D. J.; Lazo, J. S.; Roos, D. S.; Riscoe, M. K.; Phillips, M. A.; Rathod, P. K.; Van Voorhis, W. C.; Avery, V. M.; Guy, R. K. Chemical genetics of *Plasmodium falciparum*. *Nature* **2010**, *465*, 311−315.
(36) Prodromou, C.; Roe, S. M.; O'Brien, R.; Ladbury, J. E.; Piper, P. W.; Pearl, L. H. Identification and structural characterization of the ATP/ADP-binding site in the Hsp90 molecular chaperone. *Cell* **1997**, *90*, 65−75.
(37) Gallivan, J. P.; Dougherty, D. A. Cation−pi interactions in structural biology. *Proc. Natl. Acad. Sci. U. S. A.* **1999**, *96*, 9459−9464.
(38) Dutta, R.; Inouye, M. GHKL, an emergent ATPase/kinase superfamily. *Trends Biochem. Sci.* **2000**, *25*, 24−28.
(39) Grant, B. J.; Rodrigues, A. P.; ElSawy, K. M.; McCammon, J. A.; Caves, L. S. Bio3d: an R package for the comparative analysis of protein structures. *Bioinformatics* **2006**, *22*, 2695−2696.
(40) Graves, A. P.; Shivakumar, D. M.; Boyce, S. E.; Jacobson, M. P.; Case, D. A.; Shoichet, B. K. Rescoring docking hit lists for model cavity sites: Predictions and experimental testing. *J. Mol. Biol.* **2008**, *377*, 914−934.
(41) Scroggins, B. T.; Robzyk, K.; Wang, D.; Marcu, M. G.; Tsutsumi, S.; Beebe, K.; Cotter, R. J.; Felts, S.; Toft, D.; Karnitz, L.; Rosen, N.; Neckers, L. An acetylation site in the middle domain of Hsp90 regulates chaperone function. *Mol. Cell* **2007**, *25*, 151−159.
(42) Morris, G. M.; Goodsell, D. S.; Halliday, R. S.; Huey, R.; Hart, W. E.; Belew, R. K.; Olson, A. J. Automated docking using a Lamarckian genetic algorithm and an empirical binding free energy function. *J. Comput. Chem.* **1998**, *19*, 1639−1662.
(43) Morris, G. M.; Huey, R.; Lindstrom, W.; Sanner, M. F.; Belew, R. K.; Goodsell, D. S.; Olson, A. J. AutoDock4 and AutoDockTools4: automated docking with selective receptor flexibility. *J. Comput. Chem.* **2009**, *30*, 2785−2791.
(44) Panaretou, B.; Prodromou, C.; Roe, S. M.; O'Brien, R.; Ladbury, J. E.; Piper, P. W.; Pearl, L. H. ATP binding and hydrolysis are essential to the function of the Hsp90 molecular chaperone in vivo. *EMBO J.* **1998**, *17*, 4829−4836.

(45) Irwin, J. J.; Shoichet, B. K. ZINC—A free database of commercially available compounds for virtual screening. *J. Chem. Inf. Model.* **2005**, *45*, 177−182.
(46) Pettersen, E. F.; Goddard, T. D.; Huang, C. C.; Couch, G. S.; Greenblatt, D. M.; Meng, E. C.; Ferrin, T. E. UCSF chimera−A visualization system for exploratory research and analysis. *J. Comput. Chem.* **2004**, *25*, 1605−1612.
(47) Case, D. A.; Cheatham, T. E.; Darden, T.; Gohlke, H.; Luo, R.; Merz, K. M.; Onufriev, A.; Simmerling, C.; Wang, B.; Woods, R. J. The Amber biomolecular simulation programs. *J. Comput. Chem.* **2005**, *26*, 1668−1688.
(48) Harvey, M. J.; Giupponi, G.; De Fabritiis, G. ACEMD: accelerating biomolecular dynamics in the microsecond time scale. *J. Chem. Theory Comput.* **2009**, *5*, 1632−1639.
(49) Venables, W. N.; Ripley, B. D. *Modern Applied Statistics with S*, 4th ed.; Springer: New York, 2002.
(50) Sarkar, D. *Lattice: Multivariate Data Visualization with R*; Springer: New York, 2008.
(51) Humphrey, W.; Dalke, A.; Schulten, K. VMD: Visual molecular dynamics. *J. Mol. Graphics Modell.* **1996**, *14*, 33−38.
(52) Trager, W.; Jensen, J. B. Human malaria parasites in continuous culture. *Science* **1976**, *193*, 673−675.
(53) Desjardins, R. E.; Canfield, C. J.; Haynes, J. D.; Chulay, J. D. Quantitative assessment of antimalarial activity in vitro by a semiautomated microdilution technique. *Antimicrob. Agents Chemother.* **1979**, *16*, 710−718.
(54) Regalado, E. L.; Tasdemir, D.; Kaiser, M.; Cachet, N.; Amade, P.; Thomas, O. P. Antiprotozoal steroidal saponins from the marine sponge *Pandaros acanthifolium*. *J. Nat. Prod.* **2010**, *73*, 1404−1410.